Thermal and diffusion Cattaneo-Christov heat flux models on Walter's-B Buongiorno nanofluid over an electromagnetic surface with second order velocity slip.

[1*] Sathy Suresh

[1]*Assistant Professor, Vemana Institute of Technology, Bengaluru, Karnataka, India*

[1]*sathysuresh@vemanait.edu.in,*

Abstract

The intension of the current study is to explore optimization in heat transfer using Cattaneo-Christovs thermal and the solutal diffusions along with heat source/sink which are non-uniform on a stagnation points flow of nanoWalter's B fluid over an electromagnetic sheet subjected to the multiple slip mechanisms. This study also scrutinizes the role of electromagnetic fields. The flow equations are modified via incorporating suitable transformations into a self-similarity equalities. Further numerically solved by employing Runge–Kutta method of shooting technique. The acquired results shows good agreement with the previous published works. The noteworthy findings are- Walter's B nanofluid which flow parallel to the electromagnetic sheet is assisted by the Lorentz force. Electromagnetic sheet can be used for better cooling since improvement in Hartmann declines thermal boundary layer. Augmentation in thermal, velocity, and the solutal slip parameter shrink the hydrodynamic, solutal and thermal boundary layer.

Keywords: *Cattaneo-Christov, Walter's B fluid, Buongiorno nanofluid, non-uniform Heat Sink/Source, 2nd order velocity slips, concentration slip, thermal slip.*

1. Introduction.

The present technological development in the electronics industry along with the advanced energy density devices are accompanied with the thermal management encounters. It is estimated that the heat fluxs in most of these system are anticipated to go beyond 100 W/cm^2. Hence, cooling technologies containing the MCHS are continually upgraded in order to handle the associated thermal challenges. Some of these methods include usage of functionally graded materials, geometric optimization of the heat exchangers and incorporating the nanofluid as the working fluid. Nanofluid is obtained via integrating ultrafine nanoparticles comprising of mainly oxides, metals and other compounds in the heat transport fluids Recently, researchers [1-5] explored nanofluid focusing primarily on the viscosity, stability electrical and thermal performances. Buongiorno [6] suggested a nanofluid model incorporating the Brownian - thermophoresis motion properties. Recently, researchers [7-10] scrutinized the thermal conductivity behavior by incorporating Buongiorno model. In Industrial and the engineering procedures, to obtain the best quality product accurate knowledge of heat transfer procedure is very much essential. In the past most of the researchers and engineers applied Fourier's heat conduction law on order to study heat transport traits. In Recent times Liu et al. [11] and Qi and Guo [12] had a concern that Fourier's heat conduction law [13] produces parabolic energy equation thus any kind of initial disturbance would affect the whole system. Thus after the primary work of Cattaneo [14] followed by Christov [15] a new model for heat flux called Cattaneo-Christov is constituted to study heat transfer features. Currently, researchers

[16-20] explored the heat transfer nature by incorporating Cattaneo-Christov double -diffusion hypothesis over various surfaces.

No-slip condition is recurrently employed in flow of viscous fluid problems. However, in certain circumstances slip may arise at the boundary when the fluid is particulate for example suspensions, polymer, emulsions and foam solutions. Further, no-slip conditions is not valid for the flow which take place at micro and nanoscale hence, a certain degree of tangential slip should be allowed. In view of this phenomenon recently researchers [21-25] investigated flow and heat transfer by considering partial and second order slip.

Gailitis and Lielausis [26] invented a device to generate the exponentially decomposing wall-parallel Lorentz force. This device is the electromagnetic actuator containing electrodes and permanent magnet

Thus the electromagnetic body force produced due to stretching manages the flow separations and eradicate the turbulence influence developing in the flow. Researchers [27-32] investigated flow over the Riga-plate.

Through the above stated literature survey the researchers here are interested in investigating the influence of Cattaneo Christov solutal and thermal diffusions along with the non-uniform heat source-sink on the stagnation point flows of nanoWalter's B fluid over the electromagnetic sheet subjected to the slip mechanisms. The flow model are converted by incorporating self-similarity equations and then numerically handled through the Runge-Kutta shooting method.

2. Mathematical formulation.

The Present exploration deals with stagnation point flow of a Walter's B fluid over an electromagnetic sheet. Effect of Buongiorno nanofluid, Cattaneo-Christov heat along with mass flux and non-uniform heat source-sink is taken into consideration. A Cartesian coordinate system originate from leading edges of the electromagnetic sheet. The geometry of the flow problem is portrayed in Figure 1.

The boundary layer equations referring Nayak et al. [28] Shafiq et al. [31] and Ahmad et al. [27] are:

$$\frac{\partial u}{\partial x}+\frac{\partial v}{\partial y}=0 \tag{1}$$

$$u\frac{\partial u}{\partial x}+v\frac{\partial v}{\partial y}=\left(\begin{array}{l}\left(\frac{\zeta_0}{\rho_f}\right)\frac{\partial^2 u}{\partial y^2}+u_\infty\frac{\partial u_\infty}{\partial x}-\frac{k_0}{\rho_f}\left(v\frac{\partial^3 u}{\partial y^3}+u\frac{\partial^3 u}{\partial x\partial y^2}-\frac{\partial u}{\partial y}\frac{\partial^2 u}{\partial x\partial y}+\frac{\partial u}{\partial x}\frac{\partial^2 u}{\partial y^2}\right)\\ +\left(\frac{\pi j_0 M_0}{8\rho_f}\right)e^{\left(-\pi/\Lambda\right)y}\end{array}\right) \tag{2}$$

$$u\frac{\partial T}{\partial x}+v\frac{\partial T}{\partial y}+\Delta_T\begin{bmatrix} u^2\frac{\partial^2 T}{\partial x^2}+u\frac{\partial u}{\partial x}\frac{\partial T}{\partial x}+ \\ u\frac{\partial v}{\partial y}\frac{\partial T}{\partial y}+v^2\frac{\partial^2 T}{\partial y^2} \\ +v\frac{\partial u}{\partial y}\frac{\partial T}{\partial x}+v\frac{\partial v}{\partial y}\frac{\partial T}{\partial y} \\ +2uv\frac{\partial^2 T}{\partial x\partial y}\end{bmatrix}=\frac{k_f}{(\rho c_p)_f}\frac{\partial^2 T}{\partial y^2}+\begin{bmatrix}\tau D_B\frac{\partial C}{\partial y}\frac{\partial T}{\partial y}+\frac{D_T}{T_\infty}\left(\frac{\partial T}{\partial y}\right)^2+ \\ \left(\frac{ku_w(x)}{xv}\right)\begin{pmatrix}A^*(T_w-T_\infty) \\ F'(\zeta)B^*(T-T_\infty)\end{pmatrix}\end{bmatrix} \tag{3}$$

$$u\frac{\partial C}{\partial x}+v\frac{\partial C}{\partial y}+\Delta_C\begin{bmatrix} u^2\frac{\partial^2 C}{\partial x^2}+u\frac{\partial u}{\partial x}\frac{\partial C}{\partial x}+u\frac{\partial v}{\partial y}\frac{\partial C}{\partial y}+v^2\frac{\partial^2 C}{\partial y^2} \\ +v\frac{\partial u}{\partial y}\frac{\partial C}{\partial x}+v\frac{\partial v}{\partial y}\frac{\partial C}{\partial y}+2uv\frac{\partial^2 C}{\partial x\partial y}\end{bmatrix}=D_B\frac{\partial^2 C}{\partial y^2}+\frac{D_T}{T_\infty}\frac{\partial^2 T}{\partial y^2} \tag{4}$$

Boundary conditions are:

$$\text{At } y=0,\quad u=u_w(x)+A\left(\frac{\partial u}{\partial y}\right)+B\left(\frac{\partial^2 u}{\partial y^2}\right),\ v=0,\ T=T_w+L\left(\frac{\partial T}{\partial y}\right),\ C=C_w+M\left(\frac{\partial C}{\partial y}\right) \tag{5}$$

$$\text{As } y\to\infty,\ u\to u_\infty(x)=cx,\ T\to T_\infty,\quad C\to C_\infty \tag{6}$$

Here , ζ_0 is limiting viscosity at the small shear rate, k_0 is elastic parameter , j_0 is current density, g is gravitational acceleration, M_0 is magnetization of permanent magnets, k_f is thermal conductivity, l is width of electrodes and magnets, $\tau=\left(\frac{(\rho C_p)_p}{(\rho C_p)_f}\right)$ heat capacity ratios, Δ_T is thermal relaxation time, Δ_C is solutal relaxation time, D_B Brownian diffusions and D_T is thermophoretic diffusion coefficient, A, B, L, M are velocity slip constant, thermal slip constant and concentration slip constant,

In the equation (3) A^* and B^* are the coefficient of space and temperature heat source/sink and $A^*>0,\ B^*>0$ relate to the internal heat generation. $A^*<0,\ B^*<0$ Relate to internal heat absorptions.

Similar to Nayak et al. [28] , the stream function and the subsequent similarity variable considered are:

$$\left.\begin{array}{l}\psi(x,y)=x\left(\sqrt{a\upsilon_f}\right)F(\zeta),\;\;\zeta=\left(\sqrt{\dfrac{a}{\upsilon_f}}\right)y\\ u=axF'(\zeta),\;\;v=-\left(\sqrt{a\upsilon_f}\right)F(\zeta)\\ T=T_\infty+(T_w-T_\infty)\theta(\zeta),\;\;C=C_\infty+(C_w-C_\infty)\phi(\zeta)\end{array}\right\}\qquad(7)$$

ζ is non-dimensional vertical distance and $F(\zeta)$ denotes stream function,.
Thus by using (7) governing equations of motion (1)-(6) is reduced to the similarity form as:

$$\Gamma_1\frac{d^3F}{d\zeta^3}+\Gamma_2\left[2\frac{dF}{d\zeta}\frac{d^3F}{d\zeta^3}-\frac{dF}{d\zeta}\frac{d^4F}{d\zeta^4}-\left(\frac{d^2F}{d\zeta^2}\right)^2\right]+F(\zeta)\frac{d^2F}{d\zeta^2}-\left(\frac{dF}{d\zeta}\right)^2+\varepsilon^2+Ze^{-\delta\zeta}=0\qquad(8)$$

$$\frac{d^2\theta}{d\zeta^2}+\Pr\left[\begin{array}{l}(Nb)\dfrac{d\theta}{d\zeta}\dfrac{d\phi}{d\zeta}+(Nt)\left(\dfrac{d\theta}{d\zeta}\right)^2+F(\zeta)\dfrac{d\theta}{d\zeta}-\\ R_T\left(\left(\dfrac{d^2\theta}{d\zeta^2}\right)(F(\zeta))^2+F(\zeta)\dfrac{dF}{d\zeta}\dfrac{d\theta}{d\zeta}\right)\end{array}\right]+B^*\theta(\zeta)+A^*\frac{dF}{d\zeta}=0\qquad(9)$$

$$\frac{d^2\phi}{d\zeta^2}+\left(\frac{(Nt)}{(Nb)}\right)\frac{d^2\theta}{d\zeta^2}+Sc\left[F(\zeta)\frac{d\phi}{d\zeta}-R_C\left(\left(\frac{d^2\phi}{d\zeta^2}\right)(F(\zeta))^2+F(\zeta)\frac{dF}{d\zeta}\frac{d\phi}{d\zeta}\right)\right]=0\qquad(10)$$

$$\left.\begin{array}{l}\dfrac{dF(0)}{d\zeta}=1+\Upsilon_1\dfrac{d^2F(0)}{d\zeta^2}+\Upsilon_2\dfrac{d^3F(0)}{d\zeta^3},F(0)=0,\theta(0)=1+\Upsilon_3\dfrac{d\theta(0)}{d\zeta},\phi(0)=1+\Upsilon_4\dfrac{d\phi(0)}{d\zeta}\\ \dfrac{dF}{d\zeta}(\infty)=\varepsilon,\;\theta(\infty)\to 0,\;\phi(\infty)\to 0\end{array}\right\}(11)$$

Here,

$$\Gamma_1=\frac{\zeta_0}{\mu_f},\;\Gamma_2=\frac{ak_0}{\mu_f},\delta=\frac{\pi}{\Lambda\sqrt{\dfrac{a}{\upsilon_f}}},\;Z=\frac{\pi j_0Mx}{8\rho_fu_w^2},\;R_C=a\Delta_C,\;R_T=a\Delta_T,\;\varepsilon=\frac{c^2}{a^2},\Upsilon_1=A\sqrt{\frac{a}{\upsilon_f}},$$

$$Nb=\frac{(\rho c_p)_p D_B(C_w-C_\infty)}{\upsilon_f(\rho c_p)_f}\,Nt=\frac{(\rho c_p)_p D_T(T_w-T_\infty)}{\upsilon_f(\rho c_p)_f},\Upsilon_2=B\sqrt{\frac{a}{\upsilon_f}},\;\;\Upsilon_3=L\sqrt{\frac{a}{\upsilon_f}}\;\Upsilon_4=M\sqrt{\frac{a}{\upsilon_f}}$$

$$\Pr=\frac{\upsilon_f(\rho c_p)_f}{k_f},Sc={}^{\upsilon_f}\!/_{D_B}$$

Γ_1, Γ_2, Z, ε, δ, R_C R_T, Υ_1, Υ_2, Υ_3, Υ_4, Nb, Nt, $\Pr$, Sc is viscosity ratio parameter, viscoelastic parameter, Hartmann number, velocity ratio parameter, parameter signifying width of magnets and electrodes, solutal relaxation parameter, thermal relaxation parameter, first order and second

order velocity slip, thermal slip and solutal slip parameter, Brownian motion parameter, thermophoresis parameter, Prandtl number, Schmidt number.
The frictional drag $\left(C_{f_x}\right)$ is (see Qayyum et al. [30] and Hakeem et al. [35]):

$$C_{f_x} = \frac{\tau_w}{\frac{1}{2}\rho_f u_w^2} \tag{12}$$

$$\tau_w = \left[\upsilon\left(\frac{\partial u}{\partial y}\right) - k_0\left(\left(u\frac{\partial^2 u}{\partial x \partial y}\right) - \left(2\frac{\partial u}{\partial x}\frac{\partial u}{\partial y}\right)\right)\right]_{y=0}$$

Nusselt number $\left(Nu_x\right)$ is given by

$$Nu_x = \frac{x q_w}{k\left(T_w - T_\infty\right)} \tag{13}$$

$$q_w = -k\left(\frac{\partial T}{\partial y}\right)_{y=0}$$

The local Sherwood number $\left(Sh_x\right)$ is given by

$$Sh_x = \frac{x j_w}{D_B\left(C_w - C_\infty\right)} \tag{14}$$

$$j_w = -D_B\left(\frac{\partial C}{\partial y}\right)_{y=0}$$

In dimensionless form, the C_{fx}, Nu_x and Sh_x are

$$\mathrm{Re}_x^{\frac{1}{2}} C_f = 2\left(1+\Gamma_2\left(\frac{dF(0)}{d\zeta}\right)\right)\frac{d^2F(0)}{d\zeta^2},\quad Nu_x = -\frac{d\theta(0)}{d\zeta}\mathrm{Re}_x^{\frac{1}{2}}$$
$$Sh = -\frac{d\phi(0)}{d\zeta}\mathrm{Re}_x^{\frac{1}{2}} \tag{15}$$

Here, $\mathrm{Re}_x = \frac{x u_w}{v_f}$

3. Calculation

To solve numerically the nonlinear Eqs. (8) – (11) shooting method (Runge–Kutta) is implemented in the MATLAB package. Results are tabulated in Table 1-4. The achieved effects are in exceptional concurrence with the available results. (See, of Nayak et al. [28] Hakeem et al. [35], Awais et al. [34] and Nadeem et al. [33]). Physical nature of assorted variables on velocities $F'(\zeta)$, temperature $\theta(\zeta)$ and concentration $\phi(\zeta)$ are elaborated through the Figures 2-18 and in Table 4. deviation in $\left(\frac{1}{2}C_{fx}\,\mathrm{Re}_x^{1/2}\right)$ friction coefficient , $\left(\frac{1}{2}Nu_x\,\mathrm{Re}_x^{-1/2}\right)$ Nusselt number and $\left(\frac{1}{2}Sh_x\,\mathrm{Re}_x^{-1/2}\right)$ Sherwood number are addressed**.**

4. Results and discussion

Figure 2. demonstrates the influence of modified Hartmann number (Z) on the velocity profile $F'(\zeta)$. It shows that improving values of Z improves $F'(\zeta)$ hence the associated thickness of the boundary layer improves. It infers that flow in positive x-direction on the electromagnetic sheet is encouraged by the surface parallel Lorentz forces. As expected, it is observed in Figure 3. that the augmentation in Z the surface parallel Lorentz forces which has assisted the flow field decreased the temperature $\theta(\zeta)$. Hence the electromagnetic sheet can be used for better cooling effect. Temperature profiles $\theta(\zeta)$ are plotted for various values of thermal relaxation parameter (R_T) in Fig. 4. Larger values of R_T decrease the $\theta(\zeta)$ (temperature) and accompanying boundary layer thickness. In Figure 5. it is pragmatic that increment in solutal relaxation parameter (R_C) improves the concentration of the nanofluid. Through Figure 6. it is observed that improvement in the (Nb) Brownian motion parameter as anticipated enhances the temperature $\theta(\zeta)$ of the nanofluid. This is because random motion of the fluid particles generates more heat within the frame thus one can notice thermal layer thickness as Nb improves. But for larger Nb the collision among the fluid particle increase which results in depreciation of the concentration field which is revealed in Figure 7. Figure 8. and Figure9. Illustrates the influence of (Nt) thermophoresis parameter on $\theta(\zeta)$ temperature and $\phi(\zeta)$ concentration field. Larger Nt give rise to higher thermal conductivity thus there is improvement in $\theta(\zeta)$ profiles. Larger Nt initially near the boundary depreciates the concentration of the fluid but at $\zeta \geq 1.5$ concentration $\phi(\zeta)$ profiles improves. Through Figure 10. One can witness the temperature field on temperature dependent heat source-sink. As anticipated $\theta(\zeta)$ temperature in the thermal boundary layer improves with increase in A^*. Similar behavior in concentration field is noticed through Fig. 11 with increase in A^*. In Figure 12. it is detected that the boundary layer thickness $\theta(\zeta)$ declines initially near the boundary $\zeta \leq 0.5$ further improves for increase in $B^* \geq 0$. This is because improvement in internal heat generation. Figure13. Figure 14. and Figure15 signifies the influence of rising values of the δ (width of magnets and electrodes) it is perceived that enlargement in δ improves the $\theta(\zeta)$ temperature and associated boundary layer thickness and depreciates concentration and velocity of the nanofluid. Thus, for additional heating purpose thickness of magnets and electrodes could be increased. Figure 16. indicates the influence of increase in first order velocity slip Υ_1 parameter on $F'(\zeta)$ velocity profiles. It is

notified that near the boundary for $\zeta < 1$ velocity $F'(\zeta)$ and associated boundary layer thickness decreases however whenever the magnitude of Υ_1 increased far away from the boundary $\zeta \geq 1$ one can identify improvement in velocity $F'(\zeta)$ and associated boundary layer thickness. In Figure 17 and 18 one can depict the influence of Υ_3 is thermal slip parameter, Υ_4 solutal slip parameter on temperature and concentration of the nanofluid. As the magnitude of slip Υ_3 and Υ_4 improves associated boundary layer falls and there is decline in temperature and concentration of the nanofluid.

Through the Table 4. One can observe Variation in skin friction $\left(\frac{1}{2} C_{fx} \mathrm{Re}_x^{1/2}\right)$, Nusselt number $\left(\frac{1}{2} Nu_x \mathrm{Re}_x^{-1/2}\right)$ and Sherwood number $\left(\frac{1}{2} Sh_x \mathrm{Re}_x^{-1/2}\right)$ for sundry physical variables. It is evident that improvement in Z and Υ_1 improves the skin friction. Larger values of physical variables Z, R_T, R_C, A^*, B^* and Υ_4 improves heat transfer rate and $Nb, Nt, \delta, \Upsilon_1, \Upsilon_3$ declines heat transfer performance. Mass transfer performance is improved with elevating values of physical variables $Nb, Nt, A^*, B^*, \delta, \Upsilon_1, \Upsilon_3$ and Z, R_T, R_C, Υ_4 declines mass transfer rate.

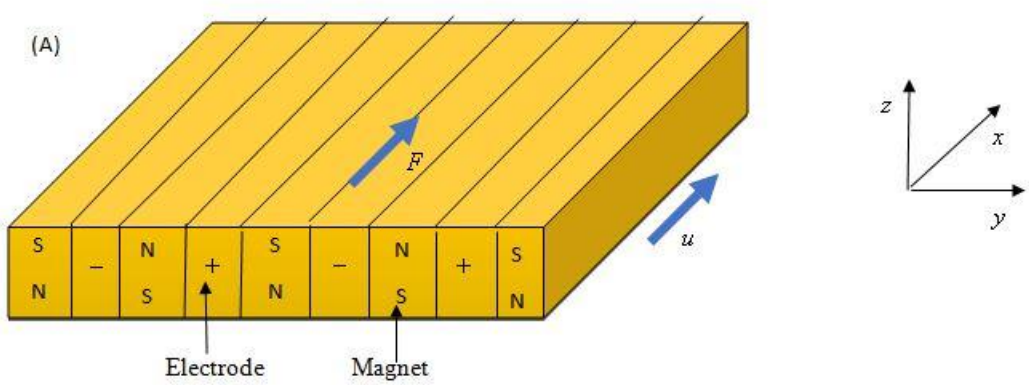

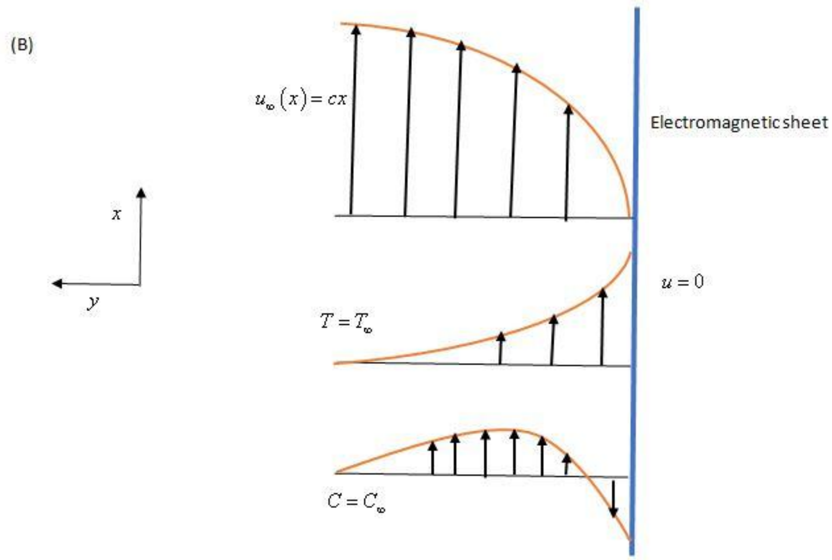

Figure1. Physical configuration of the flow problem

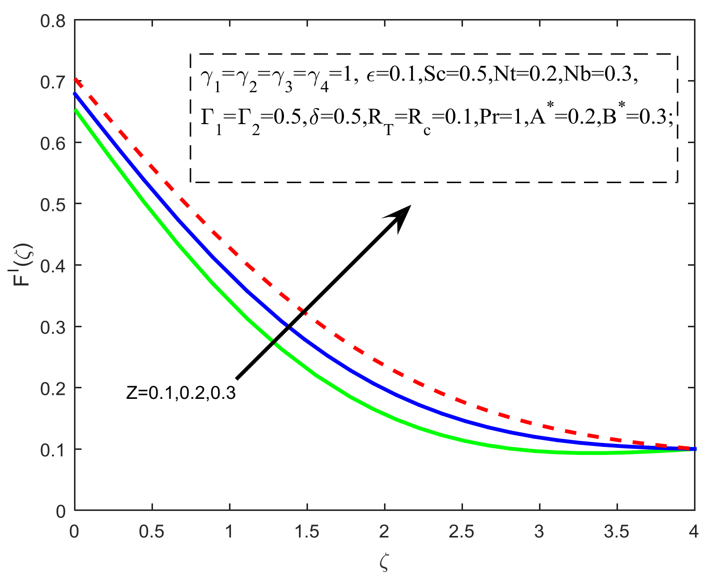

Figure 2. Influence of z on $F'(\zeta)$ velocity profile

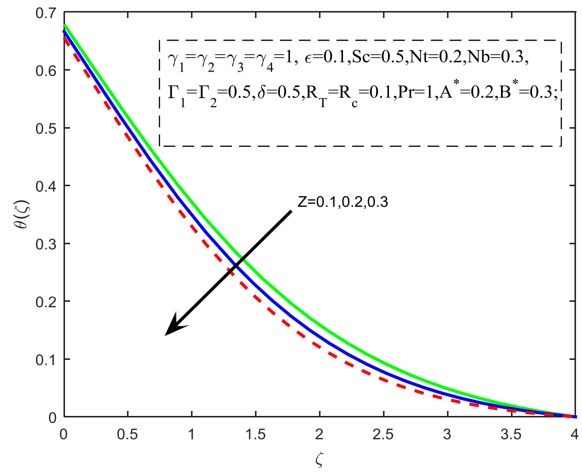

Figure 3. Influence of z on $\theta(\zeta)$ temperature profile

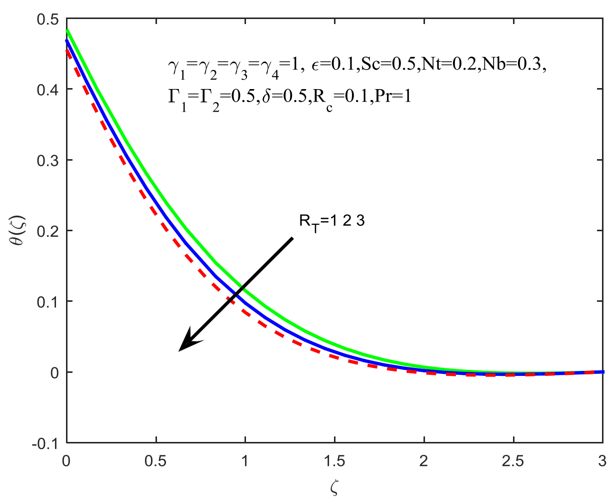

Figure 4. Influence of R_T on $\theta(\zeta)$ temperature profile

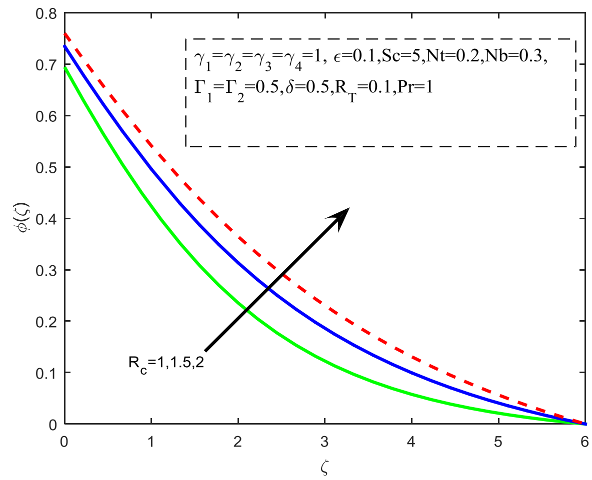

Figure 5. Influence of R_c on $\phi(\zeta)$ concentration profile

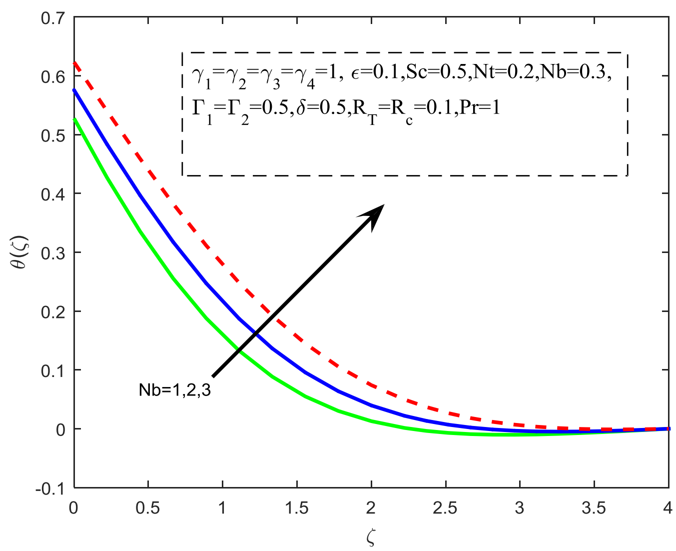

Figure 6. Influence of Nb on $\theta(\zeta)$ temperature profile

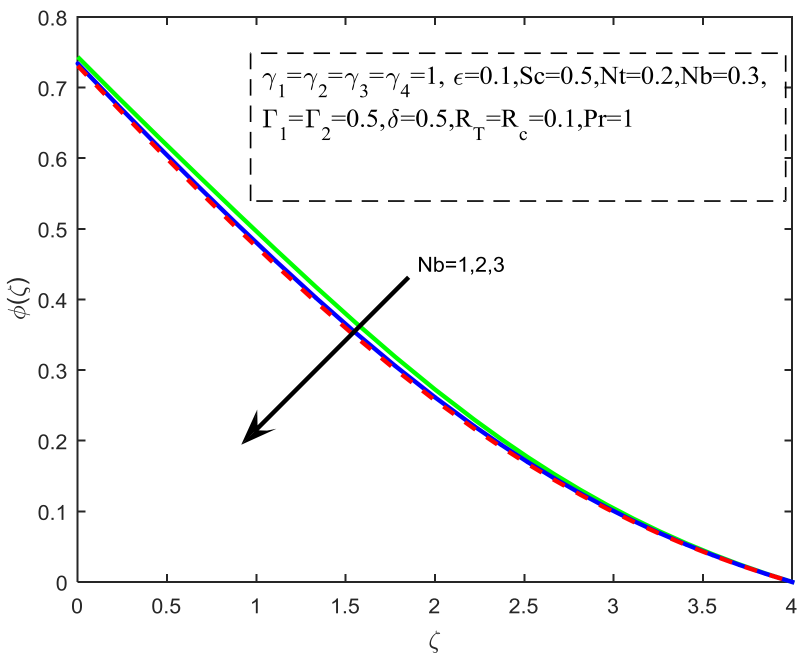

Figure 7. Influence of Nb on $\phi(\zeta)$ concentration profile

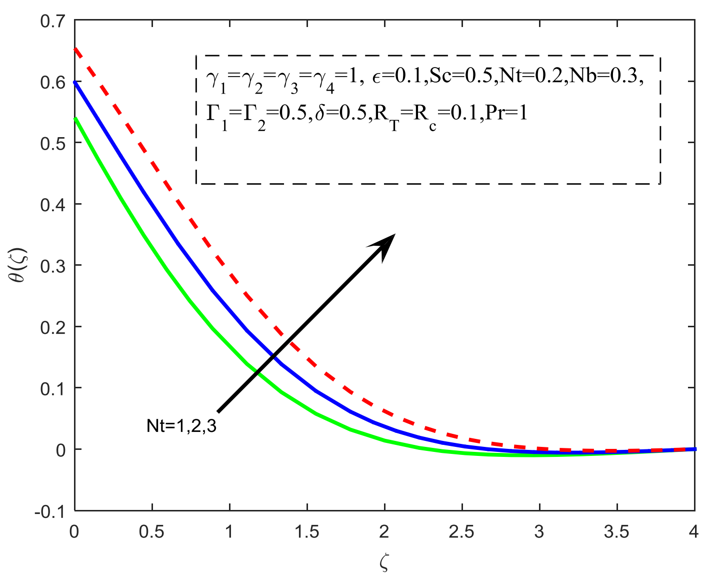

Figure 8. Influence of Nt on $\theta(\zeta)$ temperature profile

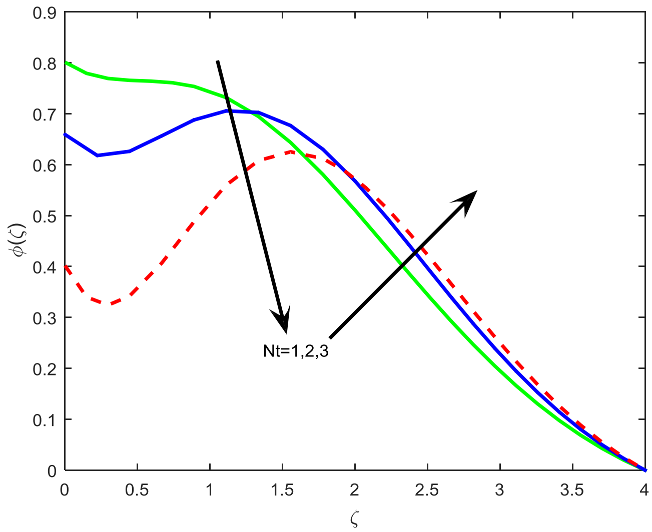

Figure 9. Influence of Nt on $\phi(\zeta)$ concentration profile

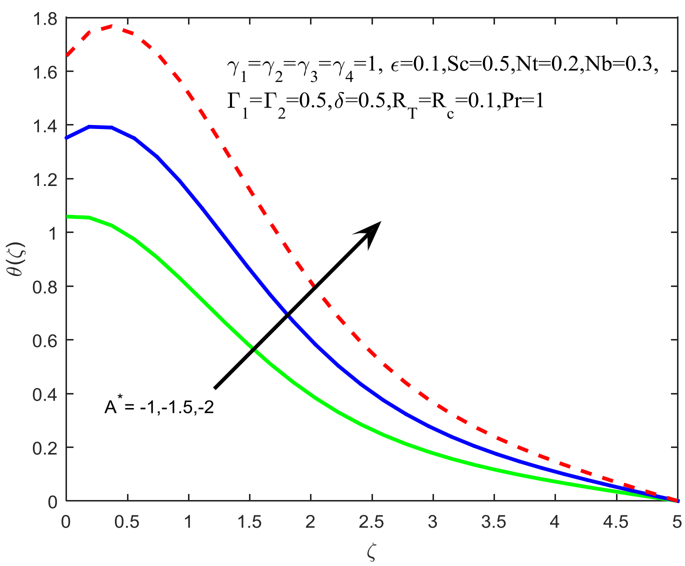

Figure 10. Influence of A^* on $\theta(\zeta)$ temperature profile

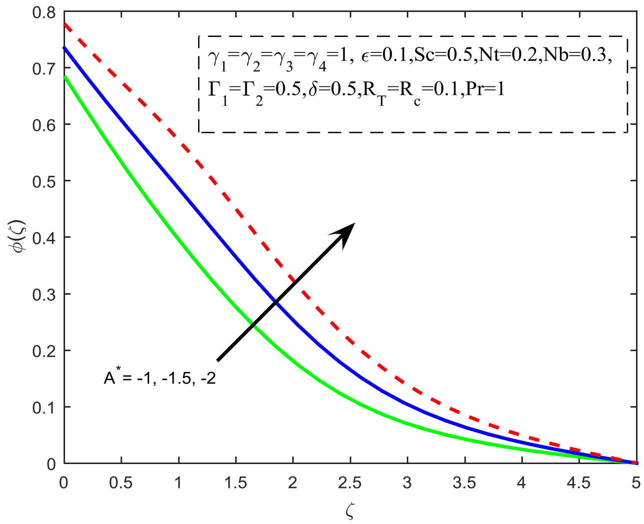

Figure 11. Influence of A^* on $\phi(\zeta)$ concentration profile

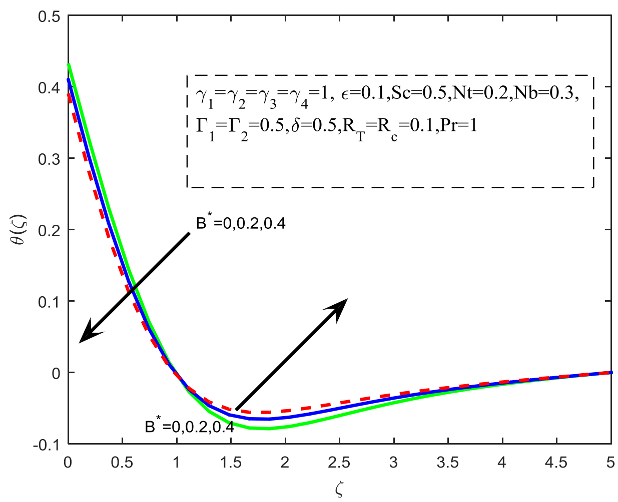

Figure 12. Influence of B^* on $\theta(\zeta)$ temperature profile

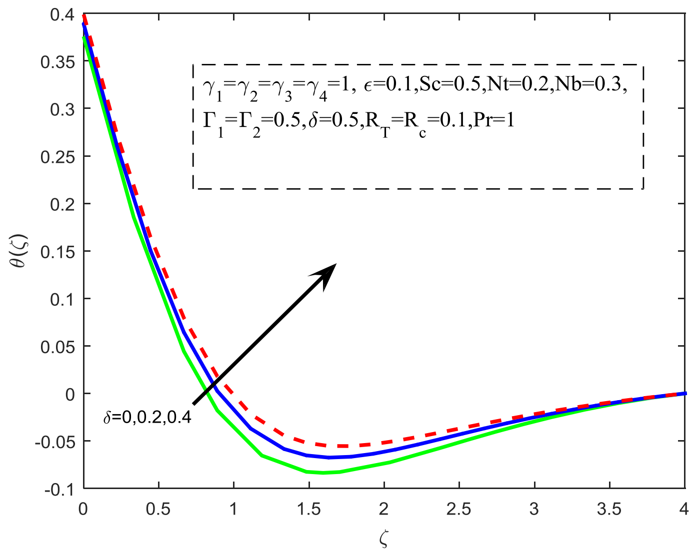

Figure 13. Influence of δ on temperature profile

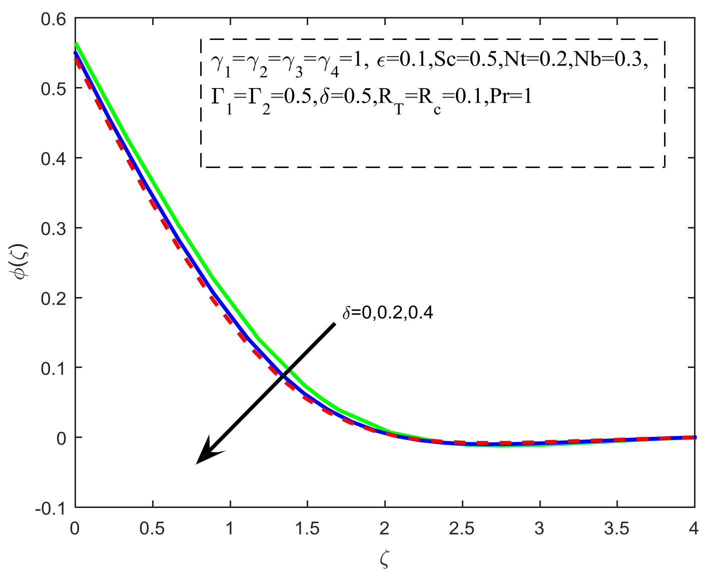

Figure 14. Influence of δ on $\phi(\zeta)$ concentration profile

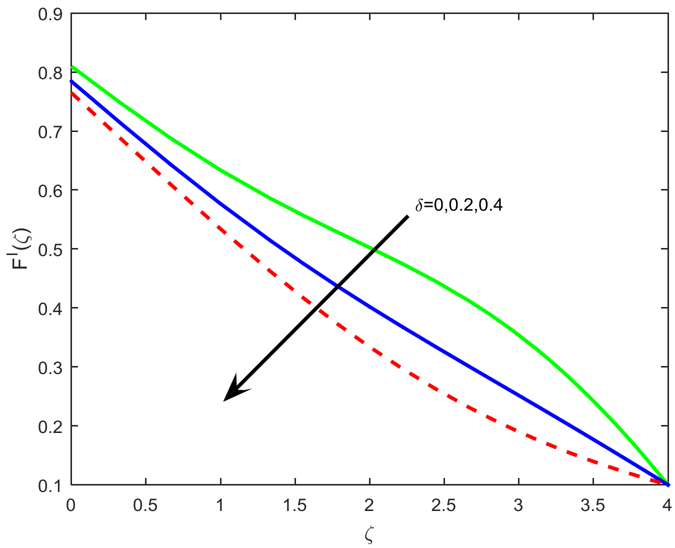

Figure 15. Influence of δ on $F'(\zeta)$ velocity profile

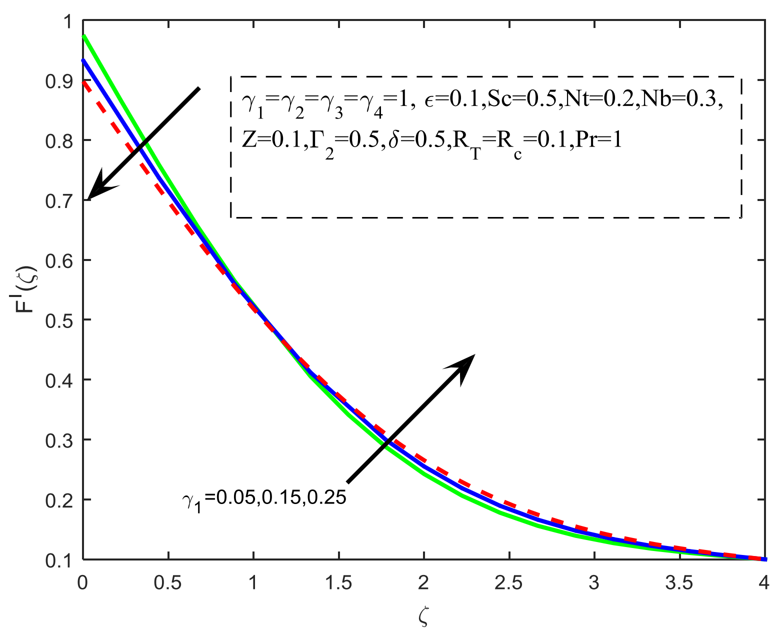

Figure 16. Influence of Υ_1 on velocity profile

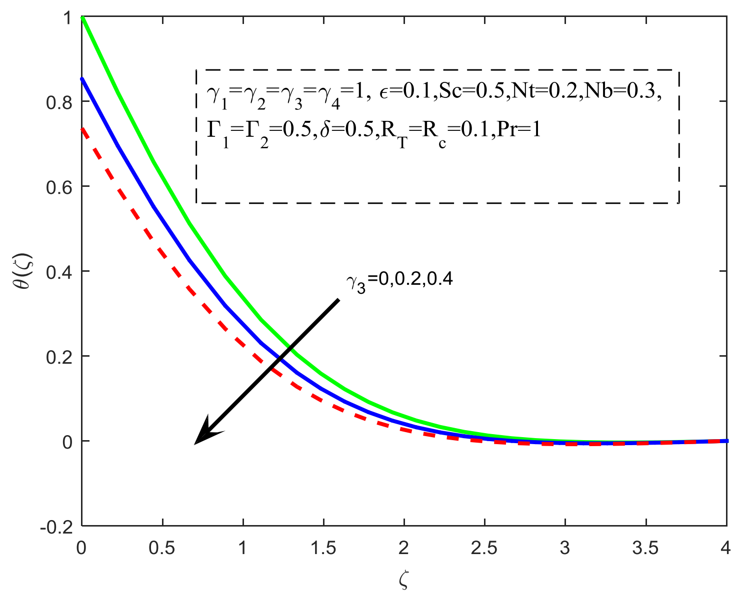

Figure 17. Influence of Υ_3 on $\theta(\zeta)$ temperature profile

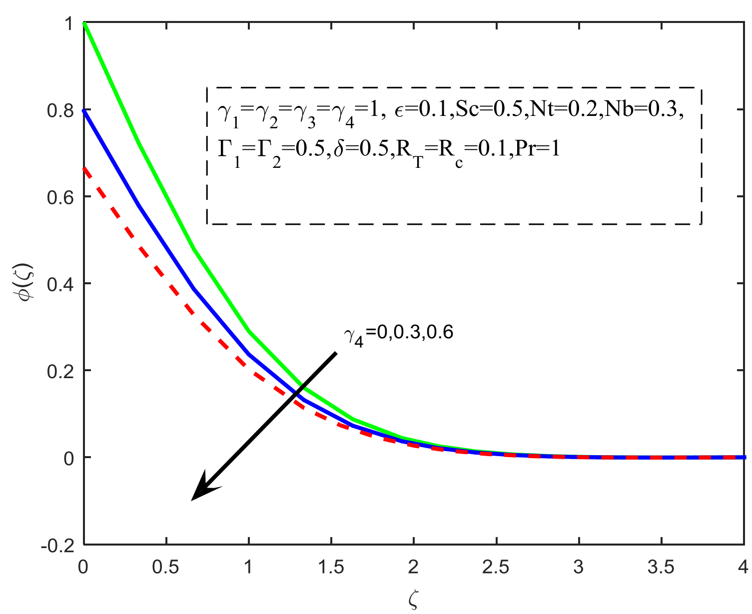

Figure 18. Influence of Υ_4 on $\phi(\zeta)$ concentration profile

Table I. Comparison values of skin friction Coefficient $\left(\frac{1}{2}C_{fx}\,\mathrm{Re}_x^{1/2}\right)$ for different values of Γ_2 when $\Upsilon_1=\Upsilon_2=\Upsilon_3=\Upsilon_4=Z=Nt=Nb=A^*=B^*=\varepsilon=R_T=R_C=0,\Pr=Sc=1$

Γ_2	Hakeem et al. [35]	Nayak et al. [28]	Present
0.3	1.19523	1.19523	1.19534
0.2	1.11803	1.11803	1.11804
0.1	1.05409	1.05409	1.05409
0.05	1.02598	1.02598	1.02598
0.01	1.00504	1.00504	1.005039
0	1.00000	1.00000	1.00000

Table II. Comparison values of local Nusselt number $\left(\frac{1}{2}Nu_x\,\mathrm{Re}_x^{1/2}\right)$ for different values of $\Pr$ when $\Upsilon_1=\Upsilon_2=\Upsilon_3=\Upsilon_4=Z=Nt=Nb=A^*=B^*=\Gamma_1=\Gamma_2=\varepsilon=R_T=R_C=0,Sc=1$

Pr	Present	Nayak et al. [28]	Awais et al. [34]
0.07	0.0665	0.0656	0.0663
0.2	0.1691	0.1691	0.1691
0.7	0.4544	0.4539	0.4534
2	0.9115	0.9114	0.9113
7	1.8954	1.8954	1.8954
20	3.3543	3.3539	3.3539

Table III. Comparison values of $\left(\frac{1}{2}C_{fx}\,\mathrm{Re}_x^{1/2}\right)$ and $\left(\frac{1}{2}Nu_x\,\mathrm{Re}_x^{1/2}\right)$ for different values of ε when

$$\Upsilon_1=\Upsilon_2=\Upsilon_3=\Upsilon_4=Z=Nt=Nb=A^*=B^*=\Gamma_2=R_T=R_C=0,\Pr=Sc=1$$

ε	$\left(\frac{1}{2}C_{fx}\,\mathrm{Re}_x^{1/2}\right)$			$\left(\frac{1}{2}Nu_x\,\mathrm{Re}_x^{1/2}\right)$		
	Present	Nayak et al. [28]	Nadeem et al. [33]	Present	Nayak et al. [28]	Nadeem et al. [33]
1	0.00000	0.00000	0.00000	0.7979	0.79788	0.79788
2	-2.0175	-2.01750	-2.01750	0.97875	0.97873	0.97873
3	-4.7293	-4.72928	-4.72928	1.13209	1.13209	1.13209
0.1	0.96938	0.96938	0.96938	0.6022	0.60216	0.60281
0.2	0.84943	0.84942	0.84942	0.6473	0.64728	0.64732
0.8	0.2994	0.29938	0.29938	0.7571	0.7571	0.75709

.

Table IV. Variation in values of $\left(\frac{1}{2}C_{fx}\,\mathrm{Re}_x^{1/2}\right)$, $\left(\frac{1}{2}Nu_x\,\mathrm{Re}_x^{-1/2}\right)$ and $\left(\frac{1}{2}Sh_x\,\mathrm{Re}_x^{-1/2}\right)$

Z	R_T	R_C	Nb	Nt	A^*	B^*	δ	Υ_1	Υ_3	Υ_4	$C_f\,\mathrm{Re}_x^{1/2}$	$Nu_x\,\mathrm{Re}_x^{-1/2}$	$Sh_x\,\mathrm{Re}_x^{-1/2}$	Elapsed Time(seconds)
0.1											-1.371024	0.321418	0.185062	0.666631
0.2											-1.295038	0.333470	0.181310	
0.3											-1.217145	0.344500	0.177636	
	1										-1.615951	0.515946	0.238104	0.693472
	2										-1.615951	0.531728	0.225539	
	3										-1.615951	0.544661	0.215339	
		1									-0.850619	0.507976	0.305900	0.737681
		1.5									-0.850619	0.509684	0.265342	
		2									-0.850619	0.510772	0.240153	
			1								-1.590979	0.472360	0.256519	0.624096
			2								-1.590979	0.424285	0.265884	
			3								-1.590979	0.376840	0.269054	
				1							-1.590979	0.459353	0.199036	0.696453
				2							-1.590979	0.401724	0.598307	
				3							-1.590979	0.346289	1.442431	
					-1						-0.851884	-0.058828	0.314556	0.884479
					-1.5						-0.851884	-0.352234	0.264695	
					-2						-0.851884	-0.657365	0.221907	
						0					-0.851884	0.567189	0.458482	0.868221
						0.2					-0.851884	0.589709	0.460556	
						0.4					-0.851884	0.609329	0.462570	
							0				-0.688593	0.624249	0.435595	0.758649
							0.2				-0.769789	0.611035	0.449909	
							0.4				-0.830111	0.601120	0.458037	
								0.05			-2.763047	0.526807	0.437537	0.728331
								0.15			-2.036706	0.516666	0.445517	
								0.25			-1.603918	0.510071	0.448880	
									0		-0.854660	0.831541	0.438390	0.678102
									0.2		-0.854660	0.735370	0.441395	
									0.4		-0.854660	0.657950	0.444218	
										0	-0.854660	0.479975	0.864147	0.777200
										0.3	-0.854660	0.487886	0.677982	
										0.6	-0.854660	0.492989	0.557805	

5. Concluding remarks

Influence of electromagnetic fields on stagnation point flow of the Walter's B nanofluid encompassing Brownian motion and the thermophoresis, Cattaneo-Christov thermal as well as solutal diffusion, non uniform heat source-sink and the multiple slip is described numerically. The foremost results of this study are:

- Walter's B nanofluid flow parallel to the electromagnetic sheet is assisted through Lorentz force.
- Enhancement in the $F'(\zeta)$ is witnessed for larger values of Z and Υ_1 this signifies that fluid velocity surpasses from the free stream velocity.
- Electromagnetic sheet can be used for better cooling since improvement in Z declines $\theta(\zeta)$.
- R_T decreases $\theta(\zeta)$ and Cattaneo-Christov thermal diffusion can be used for cooling purpose.
- Rising values of R_C and Nt improves solutal boundary layer.
- $\theta(\zeta)$ increases via larger parameter values of Nb, Nt, δ
- Improvement in B^* shows mixed performance on temperature profile.
- Improvement in Z, R_T, R_C, A^*, B^* and Υ_4 improves heat transfer rate.
- Augmentation in solutal , velocity, thermal slip and parameters shrink the hydrodynamic, thermal and solutal boundary layer.
- Mass transfer is improved with elevating values of $Nb, Nt, A^*, B^*, \delta, \Upsilon_1, \Upsilon_3$
- The average elapsed time required for computing the result is approximately 0.7 seconds.

6. References

[1]. S Mamatha Upadhya, C.S.K. Raju, S.A.Shehzad, F.M. Abbasi, "Flow of Eyring-Powell dusty fluid in a deferment of aluminum and ferrous oxide nanoparticles with Cattaneo-Christov heat flux", Powder technology..,vol.340(2018) ,pp 68-76.

[2]. C.S.K. Raju, S. Saleem, M.M.Al-Qarni, S.U. Mamatha, "Unsteady nonlinear convection on Eyring–Powell radiated flow with suspended graphene and dust particles", Microsystem Technologies.., vol.25,no4,(2019),pp 1321-1331.

[3]. S.Saleem, S.Nadeem, M.M. Rashidi, C.S.K.Raju, "An optimal analysis of radiated nanomaterial flow with viscous dissipation and heat source", Microsystem Technologies..,vol. 25,no2,(2019),pp 683-689.

[4]. M. Sheikholeslami, S. Saleem, Ahmad Shafee, Zhixiong Li, T. Hayat, A. Alsaedi, M. Ijaz Khan, "Mesoscopic investigation for alumina nanofluid heat transfer in permeable medium influenced by Lorentz forces", Computer Methods in Applied Mechanics and Engineering..,(2019),pp12-18.

[5]. S.Saleem, H. Firdous, S. Nadeem, A.U. Khan, "Convective heat and mass transfer in magneto Walter's B nanofluid flow induced by a rotating cone", Arabian Journal for Science and Engineering.., vol.44,no2,(2019),pp1515-1523.

[6]. J. Buongiorno, "Convective transport in nanofluids", ASME J. Heat Transf.., vol.128(2006),pp240-250.

[7]. C.S.K. Raju, S. Saleem, S.U. Mamatha, Iqtadar Hussain, “Heat and mass transport phenomena of radiated slender body of three revolutions with saturated porous: Buongiorno's model”, International Journal of Thermal Science..,,vol.132(2018),pp309-315.
[8]. S.T. Mohyud-Din, U. Khan, N. Ahmed, M.M. Rashidi, “A study of heat and mass transfer on magnetohydrodynamic (MHD) flow of nanoparticles”, Propulsion and Power Research.., vol.7,no.1,(2018),pp72-77.
[9]. M. Sheikholeslami, M. Jafaryar, K. Bateni, D. D. Ganji, “Two phase modeling of nanofluid flow in existence of melting heat transfer by means of HAM”, Indian Journal of Physics.., vol.92,no2, (2018),34-50.
[10]. G.K. Reddy, K. Yarrakula, C.S.K. Raju, A. Rahbari, “Mixed convection analysis of variable heat source/sink on MHD Maxwell, Jeffrey, and Oldroyd-B nanofluids over a cone with convective conditions using Buongiorno’s model”, Journal of Thermal Analysis and Calorimetry.., vol.132,no 3,(2018),pp 1995-2002.
[11]. L. Liu, L. Zheng, F. Liu, “Exact solution and invariant for fractional Cattaneo anomalous diffusion of cells in two-dimensional comb framework”, Nonlinear Dyn..,vol. 89 (2017),pp213-224.
[12]. H. Qi and X. Guo, “Transient fractional heat conduction with generalized Cattaneo model”, Int. J. Heat Mass Transf.., vol.76, (2014),pp535–539.
[13]. J. B J. Fourier ,”Theorieanalytiquede la chaleur Paris”,1822.
[14]. Cattaneo C. Sulla conduzionedelcalore, AttiSemin. Mat FisUniv Modena Reggio Emilia.., vol.3 (1948),pp 83–101.
[15]. C.I. Christov, “On frame indifferent formulation of the Maxwell-Cattaneo model of finite-speed heat conduction”, Mech. Res. Commun.., vol.36 (2009),pp 481–486. doi:10.1016/j.mechrescom.2008.11.003.
[16]. T. Hayat, M. Zubair, M. Waqas, A. Alsaedi, M. Ayub, “On stratified variable thermal conductivity stretched flow of Walter-B material subject to non-Fourier flux theory”, Neural Computing and Applications.., vol.31,no1,(2019),pp 199-205.
[17]. T. Hayat, M. Zubair, M. Waqas, A. Alsaedi, M. Ayub, “Importance of chemical reactions in flow of Walter-B liquid subject to non-Fourier flux modeling”, Journal of Molecular Liquids.., vol.238(2017),pp229-235.
[18]. S. Mamatha Upadhya, C.S.K. Raju, S. Saleem, A.A .Alderremy, “Modified Fourier heat flux on MHD flow over stretched cylinder filled with dust, Graphene and silver nanoparticles”, Results in Physics..,vol.9(2018) ,pp1377-1385.
[19]. M. Jayachandra Babu, N. Sandeep, S. Saleem, “Free convective MHD Cattaneo-Christov flow over three different geometries with thermophoresis and Brownian motion”, Alexandria Eng. J.., vol.56 (2017),pp 659–669. doi:10.1016/j.aej.2017.01.005.
[20]. S. Mamatha Upadhya, C.S.K. Raju, S. Saleem, “Nonlinear unsteady convection on micro and nanofluids with Cattaneo-Christov heat flux”, Results in Physics.., vol.9 (2018),pp 779-786.
[21]. G. S.Seth, M.K. Mishra, R. Tripathi, “MHD free convective heat transfer in a Walter’s liquid-B fluid past a convectively heated stretching sheet with partial wall slip”, Journal of the Brazilian Society of Mechanical Sciences and Engineering..,vol. 40,no2(2018),pp 103.
[22]. S.U. Mamatha, Mahesha, C.S.K. Raju, “Multiple Slips Magnetohydrodynamic Carreau Dustynano Fluid Over a Stretched Surface with Cattaneo-Christov Heat Flux” , J. Nanofluids.., vol.6 (2017),pp 1074–1081
[23]. N. Najib, N. Bachok, N. Arifin, F. Ali, “Stability Analysis of Stagnation-Point Flow in a Nanofluid over a Stretching/Shrinking Sheet with Second-Order Slip, Soret and Dufour Effects: A Revised Model”, Applied Sciences.., vol.8,no4(2018),pp 642.

[24]. S.K. Soid, S.A. Kechil, A. Ishak, "Axisymmetric stagnation-point flow over a stretching/shrinking plate with second-order velocity slip", Propulsion and Power Research.., vol.5, no3(2016),pp 194-201.

[25]. M. Rashid, M.I. Khan, T. Hayat, M.I. Khan, A. Alsaedi, "Entropy generation in flow of ferromagnetic liquid with nonlinear radiation and slip condition", Journal of Molecular Liquids.., vol.276 (2019),pp441-452.

[26]. A.K. Gailitis, O.A. Lielausis, "On the possibility of drag reduction of a flat plate in an electrolyte", Appl. Magnetohydrodyn. Trudy Inst. Fisiky AN Latvia SSR.., vol.12(1961) pp143.

[27]. R.Ahmad, M. Mustafa, M. Turkyilmazoglu, "Buoyancy effects on nanofluid flow past a convectively heated vertical Riga-plate: A numerical study", International Journal of Heat and Mass Transfer.., vol.111(2017),pp 827-835.

[28]. M.K. Nayak, I.S. Oyelakin, S. Mondal, S.S. Sen, "Impact of the Cattaneo-Christov thermal and solutal diffusion models on the stagnation point slip flow of Walters' B nanofluid past an electromagnetic sheet",Heat Transfer—Asian Research.., vol.48,no2(2019) ,pp713-726.

[29]. A.K. Hakeem, M.K.Nayak, O.D. Makinde, "Effect of Exponentially Variable Viscosity and Permeability on Blasius Flow of Carreau Nano Fluid over an Electromagnetic Plate through a Porous Medium", Journal of Applied and Computational Mechanics.., vol.5,no.2(2019),pp 390-401.

[30]. S.Qayyum, T. Hayat, S.A. Shehzad, A. Alsaedi, "Effect of a chemical reaction on magnetohydrodynamic (MHD) stagnation point flow of Walters-B nanofluid with Newtonian heat and mass conditions", Nuclear Engineering and Technology.., vol.49,no8(2017) ,pp1636-1644.

[31]. A. Shafiq, Z. Hammouch, A.Turab, "Impact of radiation in a stagnation point flow of Walters' B fluid towards a Riga plate", Thermal Science and Engineering Progress.., vol.6 (2018),pp27-33.

[32]. N. Najib, N. Bachok, N., Arifin, F. Ali, " Stability Analysis of Stagnation-Point Flow in a Nanofluid over a Stretching/Shrinking Sheet with Second-Order Slip, Soret and Dufour Effects: A Revised Model", Applied Sciences..,vol 8,no4(2018),pp642.

[33]. S. Nadeem, R. Mehmood, S.S. Motsa, "Numerical investigation on MHD oblique flow of Walter's B type nano fluid over a convective surface", International Journal of Thermal Sciences.., vol.92(2015),pp 162-172.

[34]. M. Awais, T. Hayat, A. Ali, S. Irum, "Velocity, thermal and concentration slip effects on a magneto-hydrodynamic nanofluid flow",Alexandria Engineering Journal.., vol.55,no3(2016),pp 2107-2114.

[35]. A.A. Hakeem, N.V. Ganesh, B. Ganga, "Effect of heat radiation in a Walter's liquid B fluid over a stretching sheet with non-uniform heat source/sink and elastic deformation",Journal of King Saud University-Engineering Sciences.., vol.26,no2(2014),pp168-175.